NANOPOWDERS PRODUCED FROM NATURAL SOURCES USING THE SIMPLE COPRECIPITATION METHOD

by M Munasir

ADVANCES IN NANOTECHNOLOGY

Volume 20

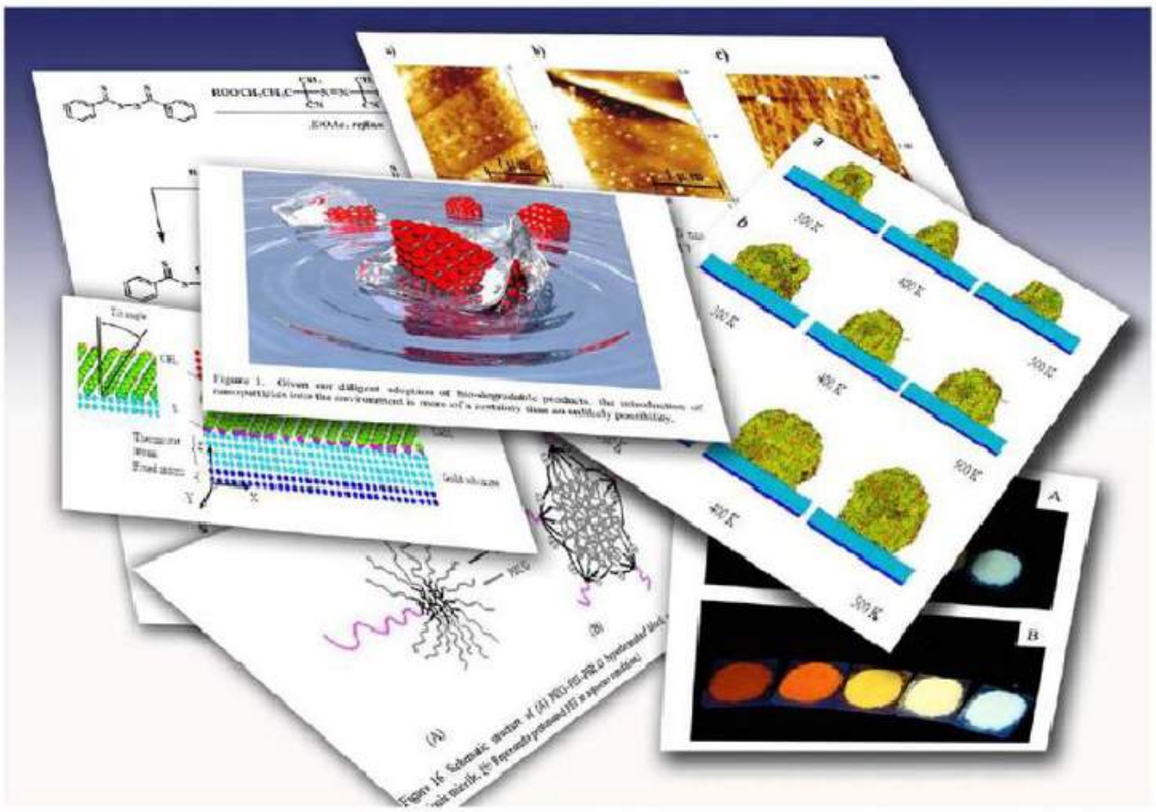

Zacharie Bartul
Jérôme Trenor
Editors

NOVA

ADVANCES IN NANOTECHNOLOGY

VOLUME 20

ADVANCES IN NANOTECHNOLOGY

Additional books in this series can be found on Nova's website under the Series tab.

Additional e-books in this series can be found on Nova's website under the eBooks tab.

ADVANCES IN NANOTECHNOLOGY

VOLUME 20

ZACHARIE BARTUL
AND
JÉRÔME TRENOR
EDITORS

nova
science publishers
New York

Library of Congress Cataloging-in-Publication Data

ISSN: 2159-1490
ISBN: 978-1-53612-903-8 (eBook)

Published by Nova Science Publishers, Inc. † New York

CONTENTS

PREFACE

In this compilation, the authors discuss nanopowders, or powders with a particle size of less than 100 nanometers. Several nanopowder types have effectively been synthesized with potential applications as follows: Fe3O4 and BaFe6O19 (as magnetic materials, microwave absorbent, magnetic fluid and gel), SiO2 (as fillers to enhance mechanical strength), and CaCO3 (as coating for corrosive protection, food additives, cosmetics and drugs). This method allows for the production of high purity nanopowders with a moderately narrow crystal size distribution and unique morphology. Next, the innovative approaches to address the lightning strikes and EMI shielding effects on composite aircraft are examined, noting that composite aircraft protection against lightning is more complex due to the anisotropic nature of composite structure and high resistance of carbon in epoxy resins. The authors go on to present results of studies of composite electrochemical coatings modified by nano- and microparticles of various natures are presented, considering the operational properties and structural features of main types of composite coatings. Later, recent advances in synthesising highly ordered Titana nanotubes are explored, with regard to selection of suitable titanium based substrate and electrolyte apart from process parameters. These parameters include temperature, pH, voltage and applications in the areas of global warming, solar energy, photocatalytic applications, biomedical starting from implants to drug-

eluding stents, sensors, and hydrogen storage. A chapter is presented on practical ways for fabricating cost-effective equipment for deposition of nanofilms, covering the most versatile techniques of sol-gel deposition and sputter-coating. The authors maintain that by applying individual ingenuity to the described frugal techniques, the reader should be able to form nanofilms of various materials with properties tailored to suit the intended application. Afterwards, the authors describe the soft, hard templated, and hierarchically ordered strategies concerning nanotechnology applied to fabricate porous carbon materials. Additionally, relevant advantages and disadvantages aim to provide the vital information about the growing field for future energy to minimize the potential environmental risks. Moving on, the authors introduce new research and related literature concerning the synthesis of cobalt diselenide ($CoSe_2$) nanoneedle arrays for efficient hydrogen evolution electrolysis. Future aspects for improving the performance of transition metal dichalcogenide-based electrocatalytic electrodes are also examined. Lastly, a study on formation of nanoporous silicon and germanium layers with silver nanoparticles by low-energy high-dose ion implantation is presented. The authors suggest ion implantation for the formation of nanoporous semiconductor thin layers, which could be easily combined with the crystalline matrix for various applications.

Chapter 1 - Nanopowders are defined as powders having a particle size less than 100 nanometers. Due to the specific surface effect, they have unique and different properties from powders with larger particle sizes. The quality of nanopowders extremely depends on the purity and homogeneity of the grain/crystallite size. These factors are associated with the complexity of how the nanopowders are prepared. Nanopowders are widely available in the form of ceramic compounds, which are generally oxides, carbonates, sulfates, and carbides. The metal-oxide ceramic nanopowders can be prepared by simple coprecipitation. This method not only can produce high purity nanopowders, but also with a relatively narrow crystal size distribution and unique morphology. Those are very crucial for any kind of application. To cite some examples, a number of nanopowder types have successfully been synthesized with potential

applications as follows: Fe_3O_4 and $BaFe_6O_{19}$ (as magnetic materials, microwave absorbent, magnetic fluid and gel), SiO_2 (as fillers to enhance mechanical strength), and $CaCO_3$ (as coating for corrosive protection, food additives, cosmetics and drugs).

Chapter 2 - This chapter reports the current state-of-the-art systems on lightning strikes, their effects on composite aircraft, and new techniques available to engineers and operators to safeguard against detrimental effects of lightning strikes. Designing and manufacturing of composite aircraft need advanced strategies to sustain the same degree of safety and shelter as achieved by conductive aluminum skinned aircrafts. Researchers and scientists have been investigating new ideas to support the development of new mitigation, diagnosis and prognosis techniques to overcome the increased challenges associated with lightning protection on composite aircraft. Lightning protection of composite aircraft is more complex due to the anisotropic nature of composite structure and high resistance of carbon in epoxy resins. A wide variety of solutions have been available for composite aircraft against lightning strike as composite materials have been expanded extensively in aircraft manufacturing during last three decades. Generally, electrically and thermally conductive materials, such as metallic foils, metal mesh, ply-integrated interwoven wires, continuous conductive path of low resistance materials and highly conductive nanoparticles and nanofilms are used to dissipate the high density current, shockwave and heat generated during the lightning strikes. This chapter deals with all the newer approaches to address the lightning strikes and EMI shielding effects on composite aircraft.

Chapter 3 - The results of studies of composite electrochemical coatings modified by nano- and microparticles of various natures are presented. Operational properties (hardness, friction coefficient, wear- and corrosion resistance, etc.) and structural features of main types of composite coatings are considered.

Chapter 4 - The chapter discusses the recent advances in synthesising highly ordered Titana nanotubes with respect to selection of suitable titanium based substrate and electrolyte apart from process parameters such as temperature, pH, voltage and also their applications in the areas of

global warming, solar energy, photocatalytic applications, biomedical starting from implants to drug-eluding stents, sensors and hydrogen storage. The superiority of electrodeposition technique over other techniques is presented. Subsequently, the chapter explains the efforts made in designing and developing titania nanotubes with considerably improved properties on different structural alloys used in aerospace applications by electrochemical anodization technique.

Chapter 5 - Nanofilms come under the category of two-dimensional nanomaterials, whose thickness lies in the range of 1nm to 100nm. Owing to their small thickness, they do not cause any appreciable change in physical dimensions or weight of the underlying substrate, but facilitate a dramatic change in its interaction with the environment. Advances in nanofilm deposition techniques have heralded breakthroughs in various areas, such as optical coatings for energy conversion and conservation, fabrication of semiconductor devices, sensors, displays and so on. Apart from their practical applications, it is only in this two-dimensional form, that the functionality of nanomaterials can be studied at a macroscopic scale, while the nanometer scale of thickness facilitates investigation of the effects of quantum confinement on various materials.

The need for exercising precise control over various process parameters generally calls for elaborate equipment for depositing nanofilms. In addition to being expensive, the deposition equipment is often optimized for some particular application and so, does not allow much room for experimentation with various parameters. This chapter describes practical ways for fabricating cost-effective equipment for deposition of nanofilms, covering the most versatile techniques of sol-gel deposition and sputter-coating. By applying individual ingenuity to the frugal techniques described in this chapter, the reader should be able to form nanofilms of various materials with properties tailored to suit the intended application.

Chapter 6 - Carbon materials mostly involved in new alternative clean and sustainable energy technologies have been playing more and more significant role in energy storage and conversion systems, especially for the carbon porous materials, because carbon porous materials with

structures can provide large surface areas for reaction, interfacial transport, or dispersion of active sites at different length scales of pores and shorten diffusion paths or reduce diffusion effect. Therefore, the soft, hard templated and hierarchically ordered strategies with nanotechnology employed to fabricate porous carbon materials are marked along with the relevant advantages and disadvantages aim to provide the vital information about the growing field for future energy to minimize the potential environmental risks.

Carbon porous materials with attractive structures as ideal candidates for the versatility and feasibility of application to energy storage and conversion should not only be realized, but also much effort has to be devoted to systematic studies on the relationship between physicochemical properties of these materials and their performances in energy conversion and storage to more efficiently stimulate further developments in this fascinating area, alongside eco-technologies that will ensure minimal environmental impact.

Chapter 7 - Hydrogen is a clean, storable, and high-energy density energy carrier, which has been considered as a promising sustainable energy alternative for meeting the global energy demand and achieving an environmentally friendly fuel economy. Whereas water splitting is one of the most promising approaches for hydrogen fuel production. As alternatives to noble metal catalyst, e.g., platinum, for the use in hydrogen evolution reaction of water splitting, transition metal dichalcogenides have shown highly potential. Furthermore, nanostructuring is an efficient method to improve the activity of heterogeneous catalysts and the performance of the electrocatalytic electrodes. Thus, this chapter aims to introduce the authors' recent research about the synthesis of cobalt diselenide ($CoSe_2$) nanoneedle arrays for efficient hydrogen evolution electrolysis, and the related literatures are briefly discussed. Finally, the future aspects for improving the performance of transition metal dichalcogenide-based electrocatalytic electrodes are also mentioned in the end of this chapter.

Chapter 8 - Experiments on formation of nanoporous silicon and germanium layers with silver nanoparticles by low-energy high-dose ion

implantation are observed. For this task Ag^{+}-ion implantation into monocrystalline silicone and germanium substrates at energy 30 keV with doses from $7.5 \cdot 10^{16}$ to $1.5 \cdot 10^{17}$ ion/cm2 was realized. Surface nanoporous semiconductor structures were studied by scanning electron microscopy, imaging and energy-dispersive X-ray analysis. It is demonstrated that nanoporous silicon and germanium with silver nanoparticles could be fabricated by Ag-ion implantation. The average sizes of porous holes and thickness of walls between porous in silicon are about 110-130 and 30-60 nm, respectively. In germanium regular holes were not observed but silver nanoparticles were smaller sizes. Thus, ion implantation is suggested to be used for a formation of naoporous semiconductor thin layers for industry, which could be easily combined with the crystalline matrix for various applications.

In: Advances in Nanotechnology. Volume 20 ISBN: 978-1-53612-902-1
Editors: Z. Bartul and J. Trenor

Chapter 1

NANOPOWDERS PRODUCED FROM NATURAL SOURCES USING THE SIMPLE COPRECIPITATION METHOD

Malik Anjelh Baqiya[1], Munasir[2], Mochamad Zainuri[1], Zaenal Arifin[1], Mashuri[1], Triwikantoro[1], Suminar Pratapa[1] and Darminto[1,*]

[1]Department of Physics, Faculty of Mathematics and Sciences, Institut Teknologi Sepuluh Nopember (ITS), Surabaya, Indonesia
[2]Department of Physics, Faculty of Mathematics and Sciences, Universitas Negeri Surabaya (UNESA), Surabaya, Indonesia

ABSTRACT

Nanopowders are defined as powders having a particle size less than 100 nanometers. Due to the specific surface effect, they have unique and different properties from powders with larger particle sizes. The quality

* Corresponding Author Email: darminto@physics.its.ac.id.

of nanopowders extremely depends on the purity and homogeneity of the grain/crystallite size. These factors are associated with the complexity of how the nanopowders are prepared. Nanopowders are widely available in the form of ceramic compounds, which are generally oxides, carbonates, sulfates, and carbides. The metal-oxide ceramic nanopowders can be prepared by simple coprecipitation. This method not only can produce high purity nanopowders, but also with a relatively narrow crystal size distribution and unique morphology. Those are very crucial for any kind of application. To cite some examples, a number of nanopowder types have successfully been synthesized with potential applications as follows: Fe_3O_4 and $BaFe_6O_{19}$ (as magnetic materials, microwave absorbent, magnetic fluid and gel), SiO_2 (as fillers to enhance mechanical strength), and $CaCO_3$ (as coating for corrosive protection, food additives, cosmetics and drugs).

Keywords: nanopowders, natural sources, coprecipitation method, Fe_3O_4, SiO_2, $CaCO_3$

INTRODUCTION

In the past few decades, many efforts have been made to investigate the structures and applications of both magnetic and non-magnetic nanomaterials. Nanomaterial has a unique feature which is different from the bulk form due to its specific surface effect. As the particle size of a nanomaterial decreases, the surface-to-volume ratio increases. Consequently, it affects the whole physical and chemical properties of the materials. For instance, the superior physical properties of nanomaterials include the improvement of mechanical, optical, electrical, and magnetic properties.

The properties of nanomaterials are generally influenced by many factors, such as particle size and shape, particle distribution and morphologies, and particle interaction with the surrounding and neighboring substances. It has been found that these factors can be modified and improved through the synthesis route, how they can be prepared. The synthesis method for obtaining nano-sized magnetic particles have been developed in various sizes and shapes [1-3]. Magnetic

nanoparticles have been widely used for biomedical applications [4-10], namely drug targeting systems [11-15], magnetic resonance imaging (MRI) [16, 17], hyperthermia [18-20], and antibacterial applications [21]. Recently, magnetic Fe_3O_4 nanoparticles have had the possibility to be used as wastewater purifiers [22]. To be applied in the biomedical fields, the nanoparticles must be non-toxic and biocompatible in organic environments. Besides, the magnetic nanoparticles should have superparamagnetic properties since they can be magnetized easily by an external magnetic field [23].

Studies of the structural and magneto-elastic properties of Fe_3O_4-based ferrofluid and hydrogel as well as their applications, employing natural iron sand as the source of raw material, have been conducted recently [24-26]. Ferrofluid is a stable colloidal suspension consisting of nano-sized magnetic particles dispersed in a liquid medium and a dispersant or surface active agent. Generally, ferrofluids can be classified into two types based on the mechanism of repulsive force among magnetic particles in a liquid medium. They are surfacted and ionic ferrofluids [27, 28]. The ion ferrofluids can be prepared by coating magnetic particles with an ionic surfactant, so that an electrostatic repulsive force occurs among the magnetic particles. Depending on the liquid acidity (pH value), the particle surface can be coated by positive or negative charges. Tetramethyl amonium hydroxide (TMAH) is one ionic surfactant having a short molecule chain. The unbound chain of TMAH can interact with the liquid medium resulting in a negative repulsive force. In the case of surfacted ferrofluids, the coated particles, by adding an oleic acid as the surfactant, have a steric repulsive force among them in a non-polar liquid medium.

One important parameter in determining various applications of ferrofluids is viscoelasticity. The basic property mainly depends on the ferrofluid's stability and magnetic properties of the dispersed particles. The stability of the magnetic particles in a ferrofluid is affected by thermal contribution [29] and equilibrium between the attraction (such as Van der Waals and dipole interactions) and the repulsion forces (steric and electrostatic interactions) among those particles [30]. Besides, the magnetic particles must be dispersed homogeneously in the liquid medium. In the

nano-sized particles, each particle domain may have three possible forms, which are primary particles, secondary particles, and a cluster of fractal aggregation. It has been found that the magnetic behavior of a ferrofluid depends not only on the primary particles, but also the secondary particles as well as the clusters formed in the ferrofluid [24]. There are only a few reports which investigate the viscoelasticity behavior of a ferrofluid. The magnetoviscous effect of ferrofluid has shown that the viscosity might change due to a significant interparticle interaction in the presence of a magnetic field [31, 32].

Another advanced application of magnetic Fe_3O_4 nanoparticles is for microwave (radar) absorbing materials [33, 34]. Additional substitution of Mn-Co in the spinel Ni-Zn ferrite has shown the best absorption characteristics with minimum reflection losses of −25 dB at 10–12 GHz [35]. Advanced materials of $(Ni_{0.65}Zn_{0.35}Fe_2O_4)_x$–$(BaFe_{12}O_{19})_{1-x}$ nano-composites have been successfully prepared exhibiting good microwave absorption properties in the X-band region [36]. Furthermore, it has been found that a composite based on polyaniline (PANI) and magnetite (Fe_3O_4) fillers can be applied for microwave absorption at the frequency range of 12.4–18 GHz (Ku-band) [37]. It is noted that the ratio of polymer matrix and magnetic fillers, the type of polymer matrix or magnetic fillers, the shape, size, and distribution of the fillers affect strongly the conductivity, dielectric, and microwave absorption properties of the final materials [37, 38]. Additionally, in the thin layered applications of radar absorbing materials, it is revealed that the thickness of the physical layers influences the absorption performance [39]. In the core-shell structure consisting Fe_3O_4 nanoparticles as a core, a strong absorption is detected at around 5 GHz [40]. Mashuri et al. [41] have successfully synthesized $Ni_{0.5}Zn_{0.5}Fe_2O_4$/Ag core-shell nanostructures employing natural iron sand consisting of a dominantly Fe_3O_4 phase. Recently, radar absorbing materials in nanostructure forms have been developed [42].

So-called hexaferrite (hexagonal ferrite) has also been intensively studied as a radar absorbing material (RAM). Regarding the ionic substitution in ferrite, it can be classified into 6 types of ferrites: M-, Z-, Y-, W-, X-, and U-type ferrites. $BaFe_{12}O_{19}$ nano-crystals, an M-type

hexaferrite, have been successfully synthesized by a modified flux method [43]. It has shown a good reflection loss in the Ku band (12.4 – 18.0 GHz) [44]. Hexaferrites with cation substitution of barium and cobalt have shown the best performance compared to the others [45].

Substitution of Co–Mn–Ti in the barium M-type hexaferrites (abbreviated as BaM) has been successfully prepared by solid state technique. The ferrites exhibit the increase of permeability and the decrease of coercivity resulting in a significant reflection loss in X-band frequencies [46, 47]. The replacement of Fe^{3+} by magnetic, non-magnetic and dielectric ions in BaM has led to a shift in the ferromagnetic resonance to lower frequencies and an increase of magnetic and dielectric losses [48]. The BaM with Co-Ti or Co-Ti-Mn substitution, namely $BaCo_xTi_xFe_{12-2x}O_{19}$ or $BaCo_xMn_xTi_{2x}Fe_{12-4x}O_{19}$, have been proven to decrease magnetic coercivity significantly, and hence, a good microwave absorption in a broad Ka bandwidth or higher frequency range has been observed [49, 50]. Besides the improvement of magnetic properties, one important key for obtaining high performance of RAM is the type of dielectric material forming a composite. The reflection loss of polyaniline (PANi)/$BaMeFe_{11}O_{19}$ composite has shown a shift to low frequencies from Ku-band to X-band [51].

Development of RAM, especially in the range of high gigahertz frequencies is crucial issue nowadays. It is very important for stealth and defense technologies. Therefore, it requires a RAM which has improved properties, such as lightweight, broad bandwidth absorption, stronger absorption, and so forth [39]. The structural, magnetic properties, and microwave absorption behaviors with different Fe/Ba mole ratio in BaM have been investigated [52, 53]. Designing a novel microwave absorber by combining three type of ferrites may result in the enhanced absorbing properties correlated to the three distinct magnetic properties [54]. The result showed a wideband single-layer microwave absorber with a satisfactory reflection loss throughout Ku-band [55]. The sample having higher magnetic susceptibility and coercivity exhibits a larger microwave absorbing ability [56]. For instance, Zn^{2+} and Mn^{2+} substituted samples have quite wide absorption bandwidths of 4 GHz at −10 dB [57]. A

microwave-absorbing paint has been coated on a conducting aluminum sheet to study the absorption characteristics of a linearly polarized TE wave at X band [58]. Systematic morphological transformation of nanoparticles on dielectric (complex permittivity and permeability) and microwave absorption properties have been estimated in X band applications (8.2–12.2 GHz) [59].

Prior to the radar absorbing applications, the synthesis and principle mechanism of BaM have been studied to improve quality and efficiency [60]. Solid based polymerization has been conducted to prepare polyaniline-barium ferrite composites. It has revealed that magnetization saturation depends on the volume fraction of ferrite in the composite, resulting in improved magnetic properties for further applications [61]. The improved electromagnetic-absorption was also observed in $BaFe_{12}O_{19}$/ZnO composites compared to the pure barium ferrite [62]. $BaMg_{0.5}Co_{0.5}Ti_{1.0}Fe_{10}O_{19}$ ferrite–acrylic resin composite has been found to be one candidate for a wideband electromagnetic compatibility and other high frequency applications [63]. In addition, the M-type hexaferrite of $BaCo^{+2}{}_{0.9}Fe^{+2}{}_{0.05}Si^{+4}{}_{0.95}Fe^{+3}{}_{10.1}O_{19}$ with 80% ferrite content in a polyurethane (PU) matrix has shown good electromagnetic or radar signal reduction [64]. Moreover, the radar absorption has also been observed in the Polypyrrole–$BaFe_{12}O_{19}$ nanocomposite due to the possible adsorption by non-magnetic ions during the polymerization process. As a result, the magnetization decreases significantly which is very important for the radar absorbing behavior [65]. The ac conductivity and the magnetic coercivity of polyaniline/$BaFe_{12}O_{19}$ composites could be enhanced and decreased, respectively, after coating with polyaniline [66]. Core–shell nano-composites of barium hexaferrite ($BaFe_{12}O_{19}$) and polyaniline have been successfully prepared by the polymerization process. It has been found that the microwave absorbing efficiency and frequency range changes with increasing the thickness of the shell [67]. Different sizes and shapes of $BaFe_{12}O_{19}$ nanoparticles have been investigated for high-frequency applications on printed electronics as well as for microwave absorption technology due to improved magnetic properties [68]. Furthermore, a

complex composite of graphene/(1−x)$BaFe_{12}O_{19}$/$CaFe_2O_4$/x$CoFe_2O_4$ ferrite is one excellent candidate for microwave absorption at 7.8–12.6 GHz [69].

Up to the present, BaM has been prepared in many methods, such as conventional ceramic techniques [70], mechanical alloying [71], carbon combustion [72], sol-gel [73, 74], sol-gel combustion [75], hydrothermal [76], and co-precipitation methods [77-79]. In order to reduce the production cost, iron sand containing mostly Fe_3O_4 phase can be used as one of the starting materials to synthesize BaM, instead of using commercial products. The study of this issue is very rare and becomes an interesting topic in advanced materials research.

Another oxide obtained from natural sand is silica (SiO_2). One chemical technique to purify the natural silica sand from inorganic and organic impurities is known as the alkalifussion method [80]. This method has been successfully employed to synthesize amorphous silica (a-SiO_2) [80] and SiO_2 crystals with different polymorphs (quartz and crystobalite phase) [81]. In the alkalifussion method, there are three steps that should be considered. The first step is preparation of sodium silicate (Na_2SiO_3) obtained by mixing the silica sand with NaOH. The second one is preparation of silicic acid ($Si(OH)_4$) obtained from the reaction between Na_2SiO_3 and HCl (strong acid) to form the silica gel. The third step is called the drying step. The precipitate of silica gel ($Si(OH)_4$) is separated from the acid solution and then dried to obtain SiO_2 powders. The coprecipitation method has also been employed to purify silica and to obtain forsterite nanopowders from natural silica sand [82]. SiO_2 nanoparticles can be used as a filler of polymeric nanocomposites for corrosive protection [83, 84]. It is known that the mechanism of anti-corrosion can be enhanced by introducing inorganic nanoparticles in the polymeric host matrix. The incorporated inorganic nanoparticles in the matrix may reduce porosity and offer a long zigzag diffusion path for corrosive agents providing better barrier protection for anti-corrosive performance [85].

Besides oxides of Fe_3O_4 and SiO_2, there is a carbonate compound that can also be obtained from natural resources, namely calcium carbonate ($CaCO_3$). In nature, $CaCO_3$ has three polymorphs. The three polymorphs

have different characteristics and physical properties; calcite, aragonite, and vaterite. The most common polymorph is calcite which is the most stable phase thermodynamically at ambient temperature and pressure. The crystal system of calcite is rhombohedral [86]. Aragonite is a metastable polymorph, which would generally change into calcite at a certain temperature and pressure. The crystal system is orthorhombic, and this polymorph has a needle-like and spindle-like shape [87]. The third polymorph is vaterite, which has a hexagonal crystal system and spherical or flower-like morphology [88, 89]. It is the rarest polymorph, unstable and usually transforming to one of the more stable forms.

The micro- and nano-sized particles of calcium carbonate have great potential for many industrial applications, such as paper [90], paint [91], and cosmetics (personal care products) [92], due to their non-toxic and biocompatible characteristics. Therefore, they can also be used in biomedical applications, such as drug delivery systems [93, 94] and tissue engineering [95]. Calcite can be used as a filler or pigment due to ease of production in a single phase. Composites containing polyvinyl alcohol as matrix, and mostly calcite and aragonite as fillers, show higher mechanical strength achieved by increasing the fillers content [96].

Several methods have been employed to synthesize $CaCO_3$ particles, such as mechanochemical processing [97], ultrasound cavitation technique [98], reverse microemulsion technique [99], ultrafine grinding [100], bubbling method [101, 102], controlled precipitation [103, 104], and carbonation of lime solutions in microemulsion systems [105] and in reverse micellar systems [106]. The formation of $CaCO_3$ polymorphs is influenced by many parameters, such as acidity (pH value) and temperature during reaction [107, 108], reactant concentration, and the presence of additives and surfactants [109-112]. $CaCO_3$ particles can be prepared from different kind of raw materials. $CaCO_3$ nanoparticles with aragonite phase have been successfully prepared from cockle shells [113, 114]. The research of the evolution of phase and morphology of precipitated $CaCO_3$ synthesized by carbonation of hydrated lime has been investigated [115]. Recently, Arifin and co-workers also have successfully prepared $CaCO_3$ particles from natural limestone by carbonation with

different and unique morphologies [116]. Natural limestone has Ca content of more than 98%, supplying $Ca(OH)_2$ solution as the starting material for the production of precipitated $CaCO_3$.

This chapter provides an intensive study on synthesis and physical characterization of Fe_3O_4, BaM, SiO_2, $CaCO_3$ and their related composites produced from natural resources using a simple coprecipitation technique. A particular application of the micro/nano-particles having unique properties is also discussed.

MATERIALS AND METHODS

Preparation of Fe_3O_4 Nanopowders and Fe_3O_4-Based Ferrofluid

Fe_3O_4 nanopowders were prepared by the coprecipitation method employing natural iron sand as the starting material. The details of the experimental process has been reported in a previous report [26]. The magnetic phase was separated using the so-called magnetic separation technique, using a permanent magnet. The magnetic iron sand was washed to remove unwanted inorganic impurities. Basically, the iron sand contains dominantly Fe_3O_4 particles. HCl and NH_4OH solutions were respectively used as dissolving and precipitating agents for the coprecipitation method as described in equations (1) and (2) [26, 117].

$$3Fe_3O_4(s) + 8HCl(l) \rightarrow 2FeCl_3(l) + FeCl_2(l) + 3H_2O(l) + 3Fe_2O_3(s) + H_2(g) \quad (1)$$

$$2FeCl_3(l) + FeCl_2(l) + 3H_2O(l) + 8NH_4OH(l) \rightarrow Fe_3O_4(s) + 8NH_4Cl(l) + 7H_2O(l) \quad (2)$$

Fe_3O_4 particles were dissolved by HCl to be $FeCl_2$ and $FeCl_3$ solution providing Fe^{2+} and Fe^{3+} ions which are very important for the formation of Fe_3O_4 phase. NH_4OH solution was added wisely to the solution to precipitate Fe_3O_4 particles. The initial acidity of the solution and the slow reaction of precipitation allows a variation of crystalline size [118]. The

precipitate was then washed by distilled water until reaching normal pH value. Black nanopowders of Fe_3O_4 were obtained after it was dried at 100°C for 1 h. TMAH was added as the ionic surfactant into the precipitate forming Fe_3O_4-based ferrofluid.

Preparation of $BaFe_{12}O_{19}$ Nanopowders and PANi/$BaFe_{12}O_{19}$ Composites

Commercial products of $BaCO_3$ powders and Fe_3O_4 nanopowders, obtained previously from iron sand, were prepared as starting materials for preparation of $BaFe_{12}O_{19}$ nanopowders via the coprecipitation method. Zn powders were used for doping of $BaFe_{12}O_{19}$ nanopowders with x = 0.3 forming $BaFe_{11.7}Zn_{0.3}O_{19}$ nanoparticles. Firstly, Fe_3O_4 nanopowders were heated at 600°C for 2 h to get Fe_2O_3 powders. Each of the powders was weighed and then dissolved by HCl solution separately. Both solutions were then mixed together using a hot plate stirrer until it reached a homogenous solution. NH_4OH solution was titrated slowly to obtain precipitated $BaFe_{12}O_{19}$ and $BaFe_{11.7}Zn_{0.3}O_{19}$. The precipitate was washed by distilled water, and then dried at 100°C for 1 h to get the sample precursors. The precursors were calcinated at 1000°C for 5 h to obtain the Barium M-type hexaferrite (BaM) phase. PANI was used as the polymeric matrix and BaM with x = 0.3 was used for the filler with volume fraction of 3 vol% coated onto a steel substrate. A casting method was applied to obtain a thick layer (4 mm) of PANI/BaM nanocomposite coating on the substrate.

Preparation of SiO_2 (Silica) Nanopowders and Al/SiO_2 Nanocomposites

In order to synthesize silica powders with high purity from natural silica sand, the magnetic phase must be removed by the magnetic

separation technique using permanent magnet. A good natural silica sand having around 65 wt% silica was used as the raw material. After the separation process, the concentration of silica increased up to 99 wt%. NaOH and HCl solutions were prepared to form sodium silicate (Na_2SiO_3) and silica gel or silicic acid ($Si(OH)_4$), respectively, as represented in equations (3) to (5) [80].

$$SiO_2(s) + 8NaOH(l) \rightarrow Na_2SiO_3(l) + H_2O(l) \quad (3)$$

$$Na_2SiO_3(l) + H_2O(l) + 2HCl(l) \rightarrow 2NaCl(s) + Si(OH)_4(l) \quad (4)$$

$$Si(OH)_4(l) \rightarrow SiO_2(s) + H_2O(l) \quad (5)$$

The use of alkali media was basically required for purifying alkali elements of the natural sand. This is called the purification step. HCl solution was slowly added to the solution until reaching a pH value of around 1-2. The silica gel, separated from NaCl, was formed allowing an easy separation of both products. For the next step, the white silica gel was washed by distilled water to remove remaining impurities, such as NaCl and acid.

Finally, the white gel was dried and calcined at certain temperatures of 900 - 950°C to obtain amorphous and crystalline silica powders, respectively. Then, the silica powders were collected for further characterization and analysis.

Al/SiO_2 nanocomposites were synthesized by the simple mixing of aluminium and SiO_2 content (in vol.%): 0, 5, and 10 with two different dispering agents, namely TMAH and n-butanol, for 2 h. The mixtures were dried at 120 °C for 12 h and then pressed in a metal dye. The samples were pre-sintered at 200°C for 0.75 h, followed by vacuum sintering at 500°C for 2 h to obtain Al/SiO_2 nanocomposites.

Preparation of $CaCO_3$ Powders and PANI/$CaCO_3$ Composite for Coating

In the production of $CaCO_3$ powders, natural limestone was used as the main raw material. It has been found that the limestone has a concentration of calcium of more than 98% based on the chemical analysis [116]. However, the magnetic separation was needed to ensure the purity of $CaCO_3$ product. $CaCO_3$ powders were synthesized by a carbonation technique using CO_2 gas flow to precipitate $CaCO_3$ as described in the former papers [116, 119].

Firstly, the extracted limestone was dissolved by distilled water at room temperature for 24 h. A clear solution of $Ca(OH)_2$ was formed. The top and bottom layers forming precipitate were removed because these layers contained impurities. Flowing CO_2 gas was conducted into the clear solution ($Ca(OH)_2$) inducing the formation of precipitate $CaCO_3$. Beside the variation of calcination temperatures, the flowing gas rate and duration were also varied in order to study the effect on the structure and morphologies of the resulted $CaCO_3$ powders.

PANi/$CaCO_3$ composites were prepared by the simple mixing method with different concentrations of $CaCO_3$ of 2.5 and 5 wt% added into the solution of dissolved PANI. A casting method was used to obtain a thick layer (about 100 μm) of PANI/$CaCO_3$ composite coatings on iron (metal). A coating of pure PANI was also prepared without the use of $CaCO_3$ particles.

Characterizations

X-ray fluorescence (XRF) analysis was performed to identify the percentage of elements in the natural sources used as the main raw material. X-ray powder diffractometry (XRD) was used to investigate the phase formation and crystal structure of the synthesized powders. The XRD was operated using CuKα source at 40 kV and 20 mA. The data were

collected from 2θ angles of 10 to 90° with the data step of 0.02. Both amorphous and crystalline phases were identified and analyzed by commercial phase identification sofware (Crystal Impact Match software) and the Rietveld method (Rietica software), respectively. The investigation of the particles' morphology was carried out by scanning electron microscopy (SEM) and tunneling electron microscopy (TEM). For the magnetic nanopowders, vibrating sample magnetometry (VSM) measurements were conducted to study the magnetic properties from magnetic hysteresis curves. VSM measurements were operated at room temperature with sweeping magnetic field from -1 to 1 T. In order to reveal microwave absorbing behavior, vector network analyzer (VNA) measurements were performed at room temperature. VNA data were collected using a wide frequency range from 10 MHz to 20 GHz. The mechanical properties were tested by standard compression apparatus in order to get modulus elasticity of the sample. The corrosion rate was measured by potentiodynamic polarization using the composites as working electrode and Ag/AgCl as reference electrode. The Tafel plots were recorded by sweeping the potential from equilibrium potential toward negative and positive potentials against Ag/AgCl reference electrodes. The electrochemical tafel slope analysis was used to evaluate the anticorrosive performance of Al/SiO_2 nanocomposites and $PANi/CaCO_3$ composite coating on stainless steel (metal) samples.

RESULTS AND DISCUSSION

Magnetoviscous Effect (MVE) of Fe_3O_4-Based Ferrofluids

Magnetic field dependence of viscosity for Fe_3O_4-TMAH ferrofluid is shown in Figure 1. Figure 1(a) shows that the viscosity increases with increasing the magnetic field for a different added volume of TMAH into the ferrofluid. The flow of ferrofluid gradually becomes slower with increasing the magnetic field because of agglomeration among Fe_3O_4 nanoparticles forming magnetic clusters, as also indicated by Ref. [120].

The increase of magnetic field results in more magnetic clusters causing more particles agglomeration [121]. Consequently, the flow of ferrofluid becomes blocked and the viscosity increases. The effects of magnetic nanoparticles concentration and the external magnetic field on the viscosity of the ferrofluid have also been investigated by previous paper [122]. The effect of temperature has also been discussed in detail [123]. It has been suggested that the magneto-viscosity is proportional to the magnetic particle content and also to the strength of magnetic field. Due to the formation of chained structures of the magnetic nanoparticles in the presence of external magnetic field (magnetic clustering), thus the viscosity increases providing the existence of shear resistance of the ferrofluid [124]. In the case of increasing added volume of TMAH, ferrofluid becomes more diluted and has a lower viscosity. The reason is that adding TMAH solution into the ferrofluid can decrease the Fe_3O_4 volume fraction of the ferrofluid resulting in the increase of distance among Fe_3O_4 nanoparticles and the decrease of interaction among them. The number of cluster and their clustering length decrease as the concentration of TMAH as surfactant increases. Therefore, the obstruction against the flow becomes less and the viscosity of ferrofluid decreases. In this case, the viscosity of the ferrofluid is determined by the concentration of carrier liquid (water) and surfactant (TMAH), hence, they influence the interaction of dispersed magnetic nanoparticles [125, 126]. In short, as can be seen in Figure 1, the MVE phenomenon depends on the concentration of the surfactant. A higher concentration of TMAH results in a lower viscosity value of the ferrofluid, indicating less viscous ferrofluids and easily to be controlled by external magnetic field. However, any changes in the viscosity influence the ferrofluid's stability.

Although the magnetoviscous behavior of the Fe_3O_4 based ferrofluid can be explained from the present results, it is necessary to confirm the viscosity data using mathematical formulations. In order to clarify the validity of magnetoviscous measurements, it is important to fit the data using theoretical studies. The equation used for this purpose is based on the Shliomis and Morozov model as written in Equation 6 [127]. To get the relative change of viscosity values against magnetic field, the derivative

form of Equation 6 is needed as shown in Equation 8. Equation 8 is derived by assuming that the rotational viscosity in the weak external magnetic field ω is equal to zero and the temperature is kept constant.

$$\Delta\eta = \frac{1}{4}\eta\phi\alpha^2 \frac{1-\omega^2\tau_B^2}{\left(1+\omega^2\tau_B^2\right)^2}, \text{ and } \alpha = \frac{\mu_o mH}{k_B T} \tag{6}$$

$$\frac{\Delta\eta}{\eta} = \frac{1}{4}\phi\left(\frac{\mu_o mH}{k_B T}\right)^2 \frac{1-\omega^2\tau_B^2}{\left(1+\omega^2\tau_B^2\right)^2} \tag{7}$$

$$\Leftrightarrow \frac{\Delta\eta}{\eta} \propto H^2 \tag{8}$$

where:

α : relation between magnetic and thermal energy
η : dynamic viscosity (kg/ms)
$\Delta\eta$: change of dynamic viscosity (kg/ms)
ω : frequency of oscilation in magnetic field (s^{-1})
τ_B : Brownian relaxation time (s)
μ_o : permeability in vacuum (Vs/Am)
ϕ : concentration of surfacted particles
m : magnetic moment of particles (Am^2)
k_B : Boltzmann constant (J/K)
T : temperature (K)
H : magnetic field (A/m)

Figure 1(b) shows the magnetic field dependence of the change of viscosity values with different concentrations of TMAH. It can be seen that the values increase linearly with increasing square magnetic field. The data were well fitted using the linear fitting from Equation 8. It is clear that ferrofluid with high TMAH concentration, namely 3 ml of TMAH

addition, shows faster viscosity change. It means that the ferrofluid is less viscous and has a relatively longer intermolecular distance. This allows small particles' interaction due to the small cohesive force among the magnetic particles in the liquid media. If there is thermal change, the energy transfer among particles is relatively low resulting in a small change of viscosity value and relative stable ferrofluid. Therefore, it is easier to control the ferrofluid under an external magnetic field.

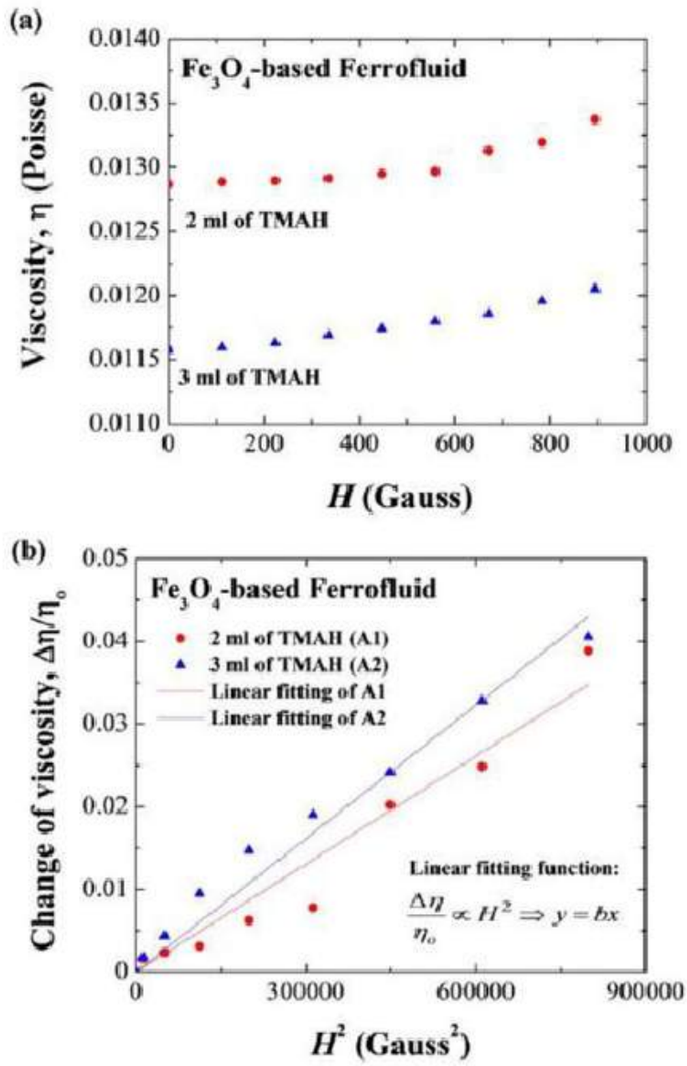

Figure 1. External magnetic field dependence on (a) viscosity of Fe_3O_4 based ferrofluids with different additional TMAH; and (b) the change of viscosity values with different concentrations of TMAH mathematically proven by Shliomis equation.

Fe_3O_4 and $BaFe_{12}O_{19}$ (BaM) as Radar Absorbing Materials (RAM)

XRD patterns of undoped BaM ($BaFe_{12}O_{19}$) and Zn-doped BaM with x = 0.3 ($BaFe_{11.7}Zn0_{.3}O_{19}$) are shown in Figure 2. The XRD analysis has revealed that the samples have BaM phase as the dominant phase and Fe_2O_3 phase as the secondary phase. The appearance of Fe_2O_3 phase is due to the existence of both Fe^{2+} and Fe^{3+} ions from Fe_3O_4 as a raw materials. During the precipitation process, Fe^{3+} ions reacted with other raw materials forming BaM phase, whereas the remaining Fe^{2+} ions reacted simultaneously forming Fe_3O_4 phase [128]. As the samples were heat treated at 1000°C, the Fe_3O_4 phase transformed into Fe_2O_3 phase as a stable form. Further analysis using the Rietveld method, gave the phase composition and lattice parameter of each sample. The refinement analysis shows that the undoped BaM has 44% of $BaFe_{12}O_{19}$ and 56% of Fe_2O_3 phase, while the doped one has 64% of $BaFe_{11.7}Zn_{0.3}O_{19}$ and 36% of Fe_2O_3 phase. For the lattice parameter, the undoped BaM has a = b = 5.88 Å and c = 23.12 Å. For Zn-doped BaM with x = 0.3, it has a = b = 5.89 Å and c = 23.21 Å. This result is consistent with the former paper [129]. The change of lattice parameters is indicated by the peak shift of the XRD pattern between the undoped and doped ones to the lower angle of 2θ in the doped sample. This is because Zn^{2+} ions as dopant substitute Fe^{3+} ions in the crystal structure. The ionic radius of the Zn^{2+} ion is larger than that of Fe^{3+} ion. Hence, the lattice parameter expands in the doped samples.

The magnetic properties of undoped and Zn-doped BaM with x = 0.3 can be studied from the hysteresis curves as shown in Figure 3. It was found that there is a decrease of magnetic coercivity and increase of magnetic saturation in the Zn-doped BaM compared to the undoped one. The decrease of coercivity in the Zn-doped BaM indicates the change of magnetic properties from hard magnetism to soft magnetism due to the substitution of Zn^{2+} ion into Fe^{3+} ion sites in the structure causing the change of magnetic domain arrangement [130]. Zn doping on Fe sites in the crystal structure gives the destruction of magnetic domain arrangement of Fe ions and the weakening of the super-exchange interactions [131]. The

soft magnetism feature simplified the mechanism of energy absorption of the electromagnetic (EM) waves, in which the energy required in the magnetization process is relatively small because the magnetic domain is easily driven by a relatively small external magnetic field. On the other hand, the increase of magnetic saturation in the doped sample is because the substitution of Zn ions into Fe sites tends to occupy the tetrahedral sites of the crystal structure rather than in the octahedral sites and this reduces the negative contribution toward the magnetic saturation [132].

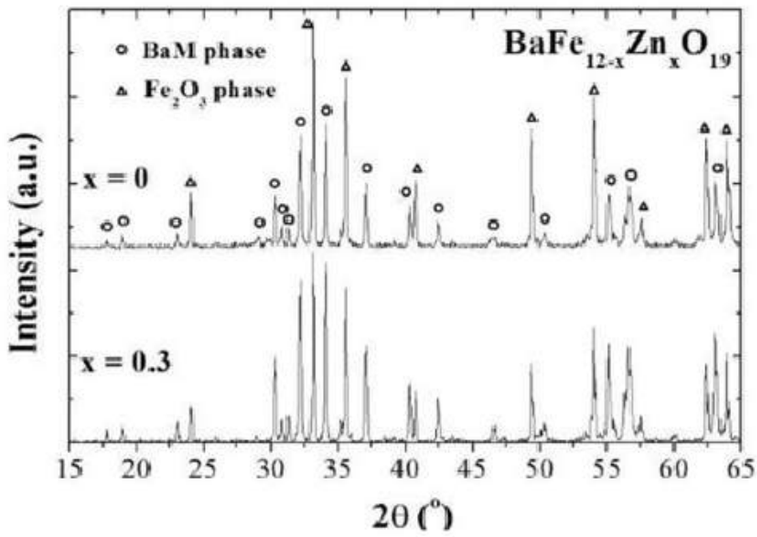

Figure 2. XRD patterns of $BaFe_{12}O_{19}$ and $BaFe_{11.7}Zn_{0.3}O_{19}$ nanoparticles synthesized by coprecipitation method using Fe_3O_4 from natural iron sand as one of the raw materials.

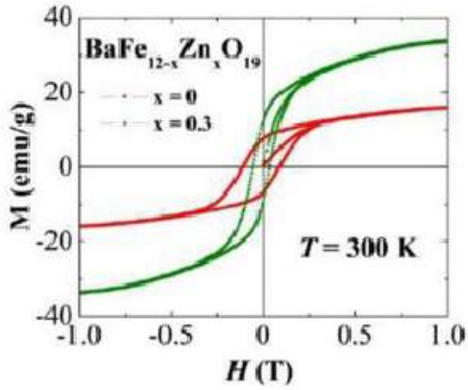

Figure 3. Magnetic hysteresis curve of $BaFe_{12}O_{19}$ and $BaFe_{11.7}Zn_{0.3}O_{19}$ nanoparticles synthesized by coprecipitation method using Fe_3O_4 from natural iron sand as one of the raw materials.

Figure 4 is presenting the information of the reflection loss against frequency at X-Ku band frequency range for single layer of PANI (P), single layer of BaM (B), and double combination layers of PANI and BaM (P-B and B-P). BaM as the magnetic filler in this present study, consists of Fe_2O_3 particles as the secondary phase. Based on Ref.[133], it has been suggested that Fe_2O_3 particles have the ability to absorb microwaves with reflection loss below the X-band frequency range. Therefore, in the present result, the existence of Fe_2O_3 is expected not to reduce the sample's ability in terms of EM waves absorption. In this research, the best reflection loss is provided by PANI – BaM (P-B) and BaM – PANI (B-P) as double layer coatings, which equals to -29.1 dB at 11.6 GHz and 30.6 dB at 17.2 GHz, respectively. This is due to the combination of absorption mechanism by BaM as the magnetic material and PANi as the conductive material. It is known that EM waves consist of two components, namely the electric field components and the magnetic field components, which are perpendicular to each other. To optimize the absorption of EM waves, this magnetic-conductive coating material must have the capability to interact with electric and magnetic fields from EM waves simultaneously resulting in better electrical loss and magnetic loss.

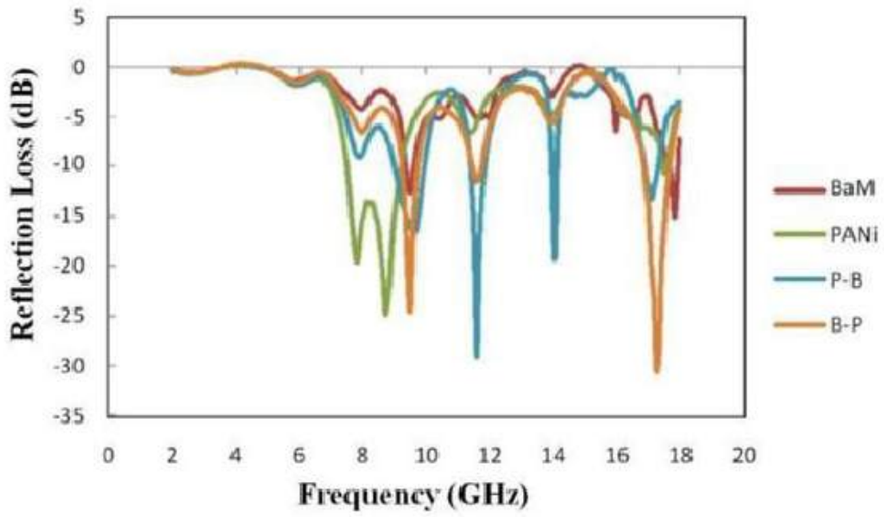

Figure 4. Reflection loss against frequency at X-Ku band frequency range for single layer PANI (P), single layer BaM (B), and combination of double layers of PANI and BaM.

Table 1. Microwave absorbing characteristics for PANI – BaM with single and double layers coating

Coating layer	Absorption band (GHz)	Absorption band width (GHz)	Reflection Loss Minimum, RL_m (dB)
BaM (B)	11.5-12.0	0.5	-5.27
	13.9-14.0	0.1	-3.02
	17.4-18.0	0.6	-15.14
PANI (P)	11.1-11.7	0.6	-6.76
	13.5-14.3	0.8	-4.70
	17.3-17.9	0.6	-10.67
P – B	11.2-12.1	0.9	-29.09
	13.8-15.0	1.2	-19.29
	16.7-17.5	0.8	-13.36
B – P	10.9-12.1	1.2	-24.47
	13.4-14.4	1.0	-5.72
	16.7-17.8	1.1	-30.63

The design of double layer coating also increases the widening of the electromagnetic wave absorption frequency, especially in the frequency range of 8 – 18 GHz as shown in detail in Table 1. The widening of the absorption band shows the effectiveness of the EM absorbing material to reduce the energy of EM waves, so that the reflected EM waves become weak. The design of double layer coating provides the combination of EM absorber materials with different capabilities and absorption characteristics on each layer, so that the wider the frequency range of EM wave absorption, the more effective it is in its application. The double layer coating offers an alternative design in addition to the use of both single layer [54, 129] and double-layer [134] of three types substitution for M-hexaferrites composites.

Silica (SiO_2) Nanopowders as Filler Reinforcement and Corrosive Protection

SiO_2 particles in the form of amorphous and crystalline can be synthesized from natural silica sand. An alkali fusion route has been

conducted to obtain amorphous SiO_2 [80] as well as SiO_2 crystals [81] using natural silica sand and sodium hydroxide with a ratio of 12.5:87.5. Basically, natural silica sand has a silicon concentration of more than 59%. Munasir et al. [81] have shown that SiO_2 powders contain quartz and cristobalite phases employing various methods. A hydrothermal technique was also performed to achieve SiO_2 powders with high purity, using a relatively high NaOH molarity of 7 M [81]. The samples were produced by immersing the sand powders with 2 M HCl for 10 h to dissolve any unwanted elements. It has been noted that a complete removal of impurities, namely calcite and microcline, results in a high purity SiO_2 from natural silica sand. The particles' morphology of the synthesized SiO_2 nanopowders is given in Figure 5. Further analysis shows an average particle size of about 20 nm.

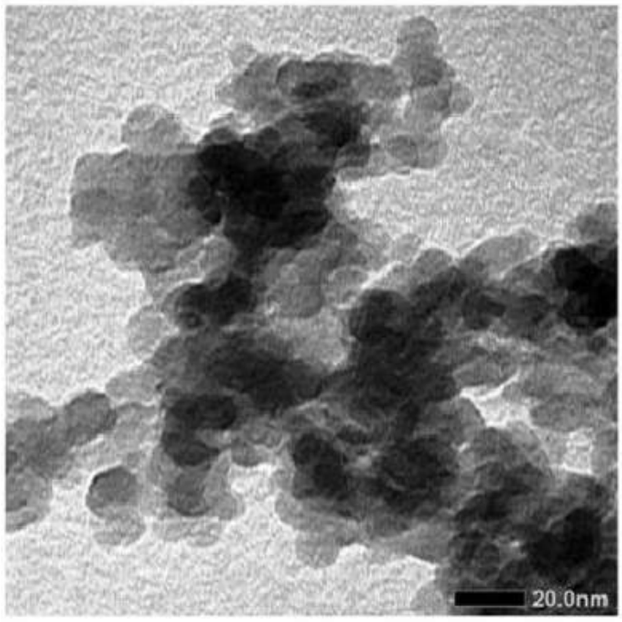

Figure 5. Nano-morphology of SiO_2 nanoparticles synthesized from natural silica sand.

In the past few years, SiO_2 nanoparticles have become a multi-functional material which can be used as nanofillers in both polymer and metal matrix nanocomposites. The nanoparticles have been widely used as a filler or reinforcer in metal matrix composites to improve the mechanical properties and corrosive protection. However, one important issue that

should be addressed regarding mechanical and anti-corrosive applications is particle distribution of filler in the matrix. This can occur due to weak interfacial bonding between fillers–matrix and particles agglomeration. In the present study, SiO_2 nanoparticles were used as filler in the aluminium matrix, forming Al/SiO_2 nanocomposite with several volume fractions of SiO_2. Generally, SiO_2 has hydrophobic properties so that interfacial bonding between the particles and host matrix is weak. In order to overcome this problem, one may add a dispersing agent, such as TMAH and n-butanol. It is expected that the dispersing agents can reduce the hydrophobicity of SiO_2 nanoparticles and improve the interfacial bonding between filler and matrix [135]. As mentioned, TMAH solution behaves as a surfactant, and hence, it also prevents agglomeration among the nanoparticles.

Table 2 presents filler volume fraction dependence of modulus elasticity and corrosion rate for Al/SiO_2 nanocomposites with the addition of TMAH and n-butanol as the dispersant. It can be seen that the mechanical properties and corrosive protection of Al/SiO_2 nanocomposites increase with increasing volume fraction of SiO_2 nanoparticles as filler, up to 5 wt%. This is because SiO_2 nanoparticles as fillers have significant influence on the mechanical properties and corrosive protection [85]. As expected, the dispering agent in the Al/SiO_2 nanocomposite can improve the interfacial bonding between aluminium and SiO_2 nanoparticles and the nano-sized fillers spread homogeneously in the aluminum matrix. Consequently, the applied mechanical stress can be distributed uniformly throughout the Al/SiO_2 nanocomposite, resulting in better mechanical strength. The proper dispersion of SiO_2 nanoparticles in the aluminium matrix also provides a barrier protection offering a long zigzag diffusion path to delay the time corrosive ions reach the inside of the nanocomposite. The current data agrees with the data of hybrid polymeric based nanocomposite coating systems observed by Sh. Ammar et al. [84], in which the coating system with 2 wt% of nano-sized SiO_2 has the best anti-corrosive performance. However, both of these performances decrease as the volume fraction of SiO_2 nanoparticles exceeds 5 wt%. This is probably

due to the particles' agglomeration in high filler volume fraction of SiO_2 nanoparticles.

Table 2. SiO_2 volume fraction dependence of corrosion rate and modulus elasticity for Al/SiO_2 nanocomposites with addition of TMAH and n-butanol as the dispersing agents

SiO_2 filler content (wt%)	Corrosion rate (mmpy)		Modulus Elasticity (GPa)	
	TMAH	n-butanol	TMAH	n-butanol
0	0.058	0.062	53.5	53.5
5	0.024	0.028	62.5	62.1
10	0.066	0.485	52.0	50.2

It can be seen in Table 2 that introducing TMAH in the Al/SiO_2 nanocomposite gives better mechanical strength and corrosive protection compared to that of introducing n-butanol as the dispersing agent. TMAH in aluminium matrix influences the formation of Al_2O_3 phase on the surface of the nanocomposite, providing additional surface protection. Hence, it is relatively stable in a corrosive atmosphere.

$CaCO_3$ Powders with Unique Morphologies and Mesopores as Fillers for Anti-Corrosion Coating

$CaCO_3$ powders with different morphologies can be synthesized from natural limestone. Based on the research of Z. Arifin et al. [119], it is revealed that the limestone contains more than 98% $CaCO_3$ with calcite phase. This is important to obtain $Ca(OH)_2$ solution with high purity for carbonation process. In this method, the formation of $CaCO_3$ phases depends strongly on experimental parameters, such as flowing rate of CO_2 gas, duration of CO_2 gas flowing, and processing temperature.

Figure 6 represents the micro-morphologies of precipitated $CaCO_3$ powders synthesized from natural limestone with different steps during carbonation process. It is found that precipitated $CaCO_3$ with vaterite phase is formed up to 50% mixed together with calcite phase at a slow flowing

rate of CO_2 gas, as in the work of Arifin et al. [119]. The vaterite phase usually precipitates in a spherical-shaped particles formed spontaneously. This result is consistent with former papers showing spherical particle morphology at slow flowing gas rate and low temperature of 70°C [88]. Flaten et al. [88] have shown that the growth of vaterite particles is influenced by the presence of monoethylene glycol as surfactant. The surfactant plays an important role in the kinetic of particle nucleation and growth. Additionally, at low gas flowing rates, only small amounts of CO_3^{2-} (derived from dissolved CO_2 gas in water) would react with Ca^{2+} (from $Ca(OH)_2$ solution). Due to the insufficient CO_3^{2-} ions and slower absorption rate of CO_2, vaterite phase is more likely to be formed, instead of calcite phase.

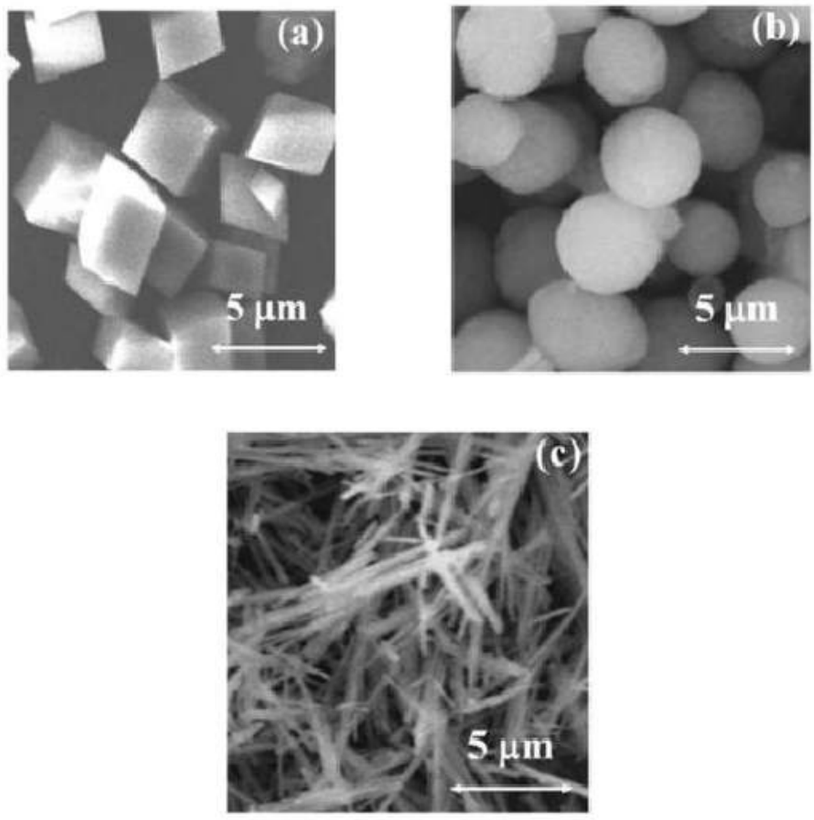

Figure 6. Micro-morphologies of precipitated $CaCO_3$ powders with different synthesis method from natural limestone resulting: (a) calcite, (b) vaterite, and (c) aragonite phases.

As the rate of flowing gas increases, the concentration of vaterite phase decreases and transforms to calcite phase. Increasing the rate of CO_2 gas flow in $Ca(OH)_2$ solution is the same as increasing CO_2 concentration in the solution. It has been found that the plate-like calcite was preferable to be formed with the increase of CO_2 concentration [136]. The concentration of calcite increased up to 100% at the rate of 10 SCFH [119]. Figure 6(a) shows $CaCO_3$ calcite particles at flowing rate of 7 SCFH. The phase transformation from vaterite to calcite is also influenced by the initial pH value and duration of CO_2 gas flow. The solution acidity is mainly determined by the $Ca(OH)_2$, as well as CO_2, concentrations. The spherical particles were formed as the initial concentration of $Ca(OH)_2$ increased up to 0.4% (m/v) [136]. At a high pH value of 12, irregular plate-block particles of vaterite and calcite phase were produced; while at the normal pH, only regular plate-block particles of calcite phase exists, as described in the work of Arifin *et al.* [119]. The value of pH might change during the carbonation process due to the formation of carbonate ion (CO_3^{2-} ions) in the solution. Therefore, it is important to consider the initial pH of the solution in obtaining the desired morphology of $CaCO_3$ particles.

Another important parameter affecting the phase formation of $CaCO_3$ particles is the processing temperature during carbonation. Arifin et al. [119] have successfully produced $CaCO_3$ particles consisting of aragonite and calcite phases with different concentrations using carbonation with a certain processing temperature. Approximately 99.2 wt% needle-like aragonite phase has been prepared by CO_2 gas flow rate of 0.5 SCFH at the relatively high temperature of 85°C. This result is in good agreement with previous reports [102, 137]. A very slow flowing gas is one important aspect to allow crystal growth in certain directions. The use of aragonite as filler in nanocomposites is for improving the mechanical properties because it has more dense particles than calcite.

PANI and its composites are multi-functional polymer-based composites which have been widely used in industrial applications, defense technology, and anticorrosive protection depending on the filler properties. For instance, a coating system of PANI/BaM hexaferrite is applied for EM wave absorbing materials, as described previously. SiO_2 and $CaCO_3$

particles as fillers in the polymeric matrix system can be applied in automotive applications and anti-corrosive coating, respectively. A. Olad and A. Rashidzadeh [138] have studied the anticorrosive behavior of PANI/$CaCO_3$ composite coating on iron samples. They have found that the composite coating with the $CaCO_3$ content of 10%w/w has the best anticorrosive performance compared to the sample without $CaCO_3$ particles as the filler. They also have shown that the efficiency of anticorrosive protection decreased with increasing $CaCO_3$ content above 20 %w/w due to the decreasing adhesion effect of composite coatings.

As mentioned, $CaCO_3$ has three polymorphs; calcite, vaterite, and aragonite phases. In this present study, it is important to investigate the influence of the different $CaCO_3$ polymorphs on the anticorrosive performance in PANI/$CaCO_3$ composite coating systems. Table 3 shows the $CaCO_3$ content dependence on the corrosion rate on PANI/$CaCO_3$ composite coatings with different polymorphs. It can be seen that PANI coating on the metal surface decreases the corrosion rate significantly. This is due to the ability to store a large quantity of charge at interface (anodic protection mechanism) provided by the PANI based coating. It means that it produces passivating layers with charge transfer reaction between the metal surface and PANI. From Table 2, it is also found that the corrosion rate decreases down to 2.5%w/w $CaCO_3$ and then increases slightly above 2.5%w/w $CaCO_3$. The presence of $CaCO_3$ particles has a significant effect on the decreasing corrosion rate because they build a long zigzag path for corrosive ions to diffuse through the composite coating before reaching the metal surface. However, increasing $CaCO_3$ content causes the increase of agglomeration and reduces the zigzag path in the coating layer. Hence, the corrosion rate increases. The increase of corrosion rate is relatively small up to 5% of $CaCO_3$ content because PANI still has a role for the passivating layer to prevent corrosive ions from penetrating the metal surface [139].

The important information in Table 3 is the effect of $CaCO_3$ polymorphs in PANI/$CaCO_3$ composite coating on metal (stainless steel) surfaces. At high $CaCO_3$ content up to 5%, it is found that the composite coating with calcite phase has relatively good stability on the corrosive

environment compared to those with vaterite and aragonite phases. This is probably because the plate-like shape of calcite particles constructs a better barrier protection with PANI against corrosive ions.

Table 3. $CaCO_3$ content dependence of corrosion rate on PANI/$CaCO_3$ composites coating on stainless steel with different polymorphs

$CaCO_3$ content (%w/w)	Corrosion rate (x 10^{-4} mmpy)				
	No coating	PANI	PANI+$CaCO_3$ Polymorph		
			PANI+ Calcite	PANI+ Vaterite+Calcite	PANI+Aragonite
0	105	30	-	-	-
2.5	-	-	1.0	1.5	2.0
5	-	-	1.5	2.5	4.0

It has also been indicated that the mesoporous $CaCO_3$ particles have potential application as good filler in the polymer based composite coating for anticorrosive applications. Further study should be considered to elucidate the anticorrosive mechanism of PANI/$CaCO_3$ composite coating with different and unique particle morphologies.

CONCLUSION

A number of nano/micropowders have been successfully synthesized from natural resources using the simple coprecipitation method, namely, Fe_3O_4 from natural iron sand, SiO_2 from natural silica sand, and $CaCO_3$ from natural limestone. We addressed general information as follows:

1. Fe_3O_4 from iron sand has been applied for magnetic gel (ferrogel), magnetic fluid (ferrofluid), and electromagnetic wave absorbing materials. The magnetic and magnetoviscosity properties of ferrofluid depend strongly on the magnetic particle size, its distribution, magnetic clustering, concentration of the magnetic nanoparticles and the amount of surfactant. The surfactant

influences the interaction of the dispersed magnetic nanoparticles affecting the stability of ferrofluid under the external magnetic field. $BaFe_{11-x}Zn_xO_{19}$ with x = 0 and 0.3 (BaM), synthesized using Fe_3O_4 as one of the raw materials, have been successfully applied as a magnetic filler in the PANI-BaM combination of single and double layer coating systems. It was found that the coating design could be used as a material candidate for EM wave absorption at the frequency range of 8 - 18 GHz.

2. SiO_2 nanoparticles as nano-sized fillers in aluminum matrix forming Al/SiO_2 nanocomposite have been successfully prepared by utilizing a dispersing agent. It was revealed that the mechanical properties and the anticorrosive behavior depend on the concentration of nanoparticles and the presence of a dispersing agent. TMAH as the dispersing agent has an important role to disperse the filler homogeneously and react with matrix forming Al_2O_3 phase at the surface to improve corrosion resistance and mechanical properties.
3. $CaCO_3$ particles with different morphologies can be produced by controlling the flowing rate of CO_2 gas and the processing temperature during the carbonation technique. These parameters control the phase formation and the particle growth. It was found that different particle morphology of $CaCO_3$ as filler in the $PANI/CaCO_3$ coating layer offers different corrosive resistance, meaning a different mechanism of anticorrosive behavior. It is suggested that the $PANI/CaCO_3$ coating layer with calcite morphology provides more stable and better anticorrosive protection.

ACKNOWLEDGMENTS

This chapter was based on research funded by several schemes of research grants, provided by LPPM ITS, DP2M – Ministry of National

Education, and DRPM – Ministry of Research, Technology and Higher Education, Republic of Indonesia, 2006 – 2016.

REFERENCES

[1] W. Wu, Q. He and C. Jiang, *Nanoscale Research Letters* 3 (11), 397-415 (2008).

[2] W. Wei, W. Zhaohui, Y. Taekyung, J. Changzhong and K. Woo-Sik, *Science and Technology of Advanced Materials* 16 (2), 023501 (2015).

[3] A. S. Teja and P.-Y. Koh, *Progress in Crystal Growth and Characterization of Materials* 55 (1–2), 22-45 (2009).

[4] T. Pedro, M. María del Puerto, V.-V. Sabino, G.-C. Teresita and J. S. Carlos, *Journal of Physics D: Applied Physics* 36 (13), R182 (2003).

[5] A. Figuerola, R. Di Corato, L. Manna and T. Pellegrino, *Pharmacological Research* 62 (2), 126-143 (2010).

[6] J. Mürbe, A. Rechtenbach and J. Töpfer, *Materials Chemistry and Physics* 110 (2–3), 426-433 (2008).

[7] P. Allia, G. Barrera, P. Tiberto, T. Nardi, Y. Leterrier and M. Sangermano, *Journal of Applied Physics* 116 (11), 113903 (2014).

[8] J. B. Mamani, L. F. Gamarra and G. E. d. S. Brito, *Materials Research* 17, 542-549 (2014).

[9] K. Onar and M. E. Yakinci, *Journal of Physics: Conference Series* 667 (1), 012005 (2016).

[10] X. Zhou, Y. Shi, L. Ren, S. Bao, Y. Han, S. Wu, H. Zhang, L. Zhong and Q. Zhang, Journal of Solid State Chemistry 196, 138-144 (2012).

[11] Y. H. Lien and T. M. Wu, *Advanced Materials Research* 47-50, 528-531 (2008).

[12] J. Chomoucka, J. Drbohlavova, D. Huska, V. Adam, R. Kizek and J. Hubalek, *Pharmacological Research* 62 (2), 144-149 (2010).

[13] O. Veiseh, J. W. Gunn and M. Zhang, *Advanced Drug Delivery Reviews* 62 (3), 284-304 (2010).

[14] P. Shao, B. Wang, Y. Wang, J. Li and Y. Zhang, *Journal of Nanomaterials* 2011 (2011).

[15] V. V. Mody, A. Cox, S. Shah, A. Singh, W. Bevins and H. Parihar, *Applied Nanoscience* 4 (4), 385-392 (2014).

[16] Y. Zhang, J.-Y. Liu, S. Ma, Y.-J. Zhang, X. Zhao, X.-D. Zhang and Z.-D. Zhang, Journal of Materials Science: *Materials in Medicine* 21 (4), 1205-1210 (2010).

[17] B. Blasiak, F. C. J. M. van Veggel and B. Tomanek, *Journal of Nanomaterials* 2013, 12 (2013).

[18] C. S. S. R. Kumar and F. Mohammad, *Advanced Drug Delivery Reviews* 63 (9), 789-808 (2011).

[19] S. Laurent, S. Dutz, U. O. Häfeli and M. Mahmoudi, *Advances in Colloid and Interface Science* 166 (1–2), 8-23 (2011).

[20] L. Pham Hoai, T. Pham Van, T. Nguyen Anh, T. Nguyen Chi, M. Do Hung, P. Nguyen Xuan and H. Le Van, *Journal of Physics: Conference Series* 187 (1), 012069 (2009).

[21] Y. T. Prabhu, K. V. Rao, B. S. Kumari, V. S. S. Kumar and T. Pavani, *International Nano Letters* 5 (2), 85-92 (2015).

[22] Y. F. Shen, J. Tang, Z. H. Nie, Y. D. Wang, Y. Ren and L. Zuo, *Separation and Purification Technology* 68 (3), 312-319 (2009).

[23] M. Mahmoudi, S. Sant, B. Wang, S. Laurent and T. Sen, *Advanced Drug Delivery Reviews* 63 (1–2), 24-46 (2011).

[24] A. Taufiq, Sunaryono, E. G. Rachman Putra, S. Pratapa and Darminto, *Materials Science Forum* 827, 213-218 (2015).

[25] Sunaryono, A. Taufiq, E. G. R. Putra, A. Okazawa, I. Watanabe, N. Kojima, S. Rugmai, S. Soontaranon, M. Zainuri, Triwikantoro, S. *Pratapa and Darminto, Nano* 11 (03), 1650027 (2016).

[26] Triwikantoro, M. A. Baqiya, T. Heriyanto, Mashuri and Darminto, *Journal of Superconductivity and Novel Magnetism* 30, 555-560 (2017).

[27] J. Li, X. Qiu, Y. Lin, X. Liu, R. Gao and A. Wang, *Applied Surface Science* 256 (23), 6977-6981 (2010).

[28] L. Rodríguez-Arco, M. T. López-López, F. González-Caballero and J. D. G. Durán, *Journal of Colloid and Interface Science* 357 (1), 252-254 (2011).

[29] M. Alsaady, R. Fu, B. Li, R. Boukhanouf and Y. Yan, *Applied Thermal Engineering* 88, 14-21 (2015).

[30] E. Krutikova and A. O. Ivanov, Physics Procedia 9, 49-53 (2010).

[31] S. Odenbach, L. M. Pop and A. Y. Zubarev, *GAMM-Mitteilungen* 30 (1), 195-204 (2007).

[32] J. M. Linke and S. Odenbach, *Journal of Magnetism and Magnetic Materials* 396, 85-90 (2015).

[33] M. Jazirehpour and S. A. Seyyed Ebrahimi, *Journal of Alloys and Compounds* 638, 188-196 (2015).

[34] N. Shibing, L. Shumei, P. Qingtao, Y. Feng, H. Kai and H. Deyan, *Journal of Physics D: Applied Physics* 42 (5), 055004 (2009).

[35] H. Sözeri, F. Genç, B. Ünal, A. Baykal and B. Aktaş, *Journal of Alloys and Compounds* 660, 324-335 (2016).

[36] S. Hazra, B. K. Ghosh, M. K. Patra, R. K. Jani, S. R. Vadera and N. N. Ghosh, *Powder Technology* 279, 10-17 (2015).

[37] B. Belaabed, J. L. Wojkiewicz, S. Lamouri, N. El Kamchi and T. Lasri, *Journal of Alloys and Compounds* 527, 137-144 (2012).

[38] J. C. Aphesteguy, A. Damiani, D. DiGiovanni and S. E. Jacobo, *Physica B: Condensed Matter* 407 (16), 3168-3171 (2012).

[39] F. M. Idris, M. Hashim, Z. Abbas, I. Ismail, R. Nazlan and I. R. Ibrahim, *Journal of Magnetism and Magnetic Materials* 405, 197-208 (2016).

[40] Y. Li, G. Chen, Q. Li, G. Qiu and X. Liu, *Journal of Alloys and Compounds* 509 (10), 4104-4107 (2011).

[41] Mashuri, Triwikantoro, E. Yahya and Darminto, *AIP Conference Proceedings* 1284 (1), 113-117 (2010).

[42] Y. Wang, T. Li, L. Zhao, Z. Hu and Y. Gu, *Energy and Power Engineering* 3 (4), 580-584 (2011).

[43] B. C. Brightlin and S. Balamurugan, *Journal of Superconductivity and Novel Magnetism*, 1-11 (2016).

[44] R. Sharma, R. C. Agarwala and V. Agarwala, *Materials Letters* 62 (15), 2233-2236 (2008).

[45] R. C. Pullar, *Progress in Materials Science* 57 (7), 1191-1334 (2012).

[46] S. P. Gairola, V. Verma, A. Singh, L. P. Purohit and R. K. Kotnala, *Solid State Communications* 150 (3–4), 147-151 (2010).

[47] P. Meng, K. Xiong, K. Ju, S. Li and G. Xu, *Journal of Magnetism and Magnetic Materials* 385, 407-411 (2015).

[48] H. Sözeri, Z. Mehmedi, H. Kavas and A. Baykal, *Ceramics International* 41 (8), 9602-9609 (2015).

[49] C. Dong, X. Wang, P. Zhou, T. Liu, J. Xie and L. Deng, *Journal of Magnetism and Magnetic Materials* 354, 340-344 (2014).

[50] S. Choopani, N. Keyhan, A. Ghasemi, A. Sharbati and R. S. Alam, *Materials Chemistry and Physics* 113 (2–3), 717-720 (2009).

[51] T. B. Ghzaiel, W. Dhaoui, F. Schoenstein, P. Talbot and F. Mazaleyrat, *Journal of Alloys and Compounds* (2016).

[52] S. Verma, S. K. Dhawan, A. Paesano Jr, O. P. Pandey and P. Sharma, *Journal of Magnetism and Magnetic Materials* 396, 308-312 (2015).

[53] M. Yazan, H. M. Sami, A. Ahmad and N. A. Aynour, IOP *Conference Series: Materials Science and Engineering* 92 (1), 012019 (2015).

[54] S. S. S. Afghahi, M. Jafarian and Y. Atassi, *Journal of Magnetism and Magnetic Materials* 419, 62-67 (2016).

[55] M. K. Tehrani, A. Ghasemi, M. moradi and R. S. Alam, *Journal of Alloys and Compounds* 509 (33), 8398-8400 (2011).

[56] A. Ghasemi, A. Hossienpour, A. Morisako, A. Saatchi and M. Salehi, *Journal of Magnetism and Magnetic Materials* 302 (2), 429-435 (2006).

[57] H. Sözeri, H. Deligöz, H. Kavas and A. Baykal, *Ceramics International* 40 (6), 8645-8657 (2014).

[58] M. R. Meshram, N. K. Agrawal, B. Sinha and P. S. Misra, *Journal of Magnetism and Magnetic Materials* 271 (2–3), 207-214 (2004).

[59] S. Tyagi, H. B. Baskey, R. C. Agarwala, V. Agarwala and T. C. Shami, *Ceramics International* 37 (7), 2631-2641 (2011).

[60] Y. Liu, M. G. B. Drew and Y. Liu, *Materials Chemistry and Physics* 134 (1), 266-272 (2012).

[61] T. Ben Ghzaiel, W. Dhaoui, A. Pasko and F. Mazaleyrat, *Materials Chemistry and Physics* 179, 42-54 (2016).

[62] W. Chen, J. Zheng and Y. Li, *Journal of Alloys and Compounds* 513, 420-424 (2012).

[63] R. Shams Alam, M. Kavosh Tehrani, M. Moradi, E. Hosseinpour and A. Sharbati, *Journal of Magnetism and Magnetic Materials* 323 (8), 1040-1043 (2011).

[64] S. M. Abbas, A. K. Dixit, R. Chatterjee and T. C. Goel, *Journal of Magnetism and Magnetic Materials* 309 (1), 20-24 (2007).

[65] B. Birsöz, A. Baykal, H. Sözeri and M. S. Toprak, *Journal of Alloys and Compounds* 493 (1–2), 481-485 (2010).

[66] J. Jiang, L.-H. Ai, D.-B. Qin, H. Liu and L.-C. Li, *Synthetic Metals* 159 (7–8), 695-699 (2009).

[67] J. Liu, J. Zhang, Y. Li and M. Zhang, *Materials Chemistry and Physics* 163, 470-477 (2015).

[68] S. Myllymäki, M. Maček Kržmanc, M. Sloma, J. Juuti, M. Nelo, M. Teirikangas, M. Jakubowska, D. Suvorov and H. Jantunen, *Journal of Magnetism and Magnetic Materials* 419, 218-224 (2016).

[69] H. Yang, T. Ye, Y. Lin, J. Zhu and F. Wang, *Journal of Alloys and Compounds* 683, 567-574 (2016).

[70] Y. Yang, F. Wang, X. Liu, J. Shao and D. Huang, *Journal of Magnetism and Magnetic Materials* 421, 349-354 (2017).

[71] P. Sharma, R. A. Rocha, S. N. de Medeiros and A. Paesano Jr, *Journal of Alloys and Compounds* 443 (1–2), 37-42 (2007).

[72] K. S. Martirosyan, E. Galstyan, S. M. Hossain, Y.-J. Wang and D. Litvinov, *Materials Science and Engineering:* B 176 (1), 8-13 (2011).

[73] L. Dong, Z. Han, Y. Zhang, Z. Wu and X. Zhang, *Rare Metals* 25 (6), 605-608 (2006).

[74] S. K. Chawla, R. K. Mudsainiyan, S. S. Meena and S. M. Yusuf, *Journal of Magnetism and Magnetic Materials* 350, 23-29 (2014).

[75] Y. Y. Meng, M. H. He, Q. Zeng, D. L. Jiao, S. Shukla, R. V. Ramanujan and Z. W. Liu, *Journal of Alloys and Compounds* 583, 220-225 (2014).

[76] M. Drofenik, I. Ban, D. Makovec, A. Žnidaršič, Z. Jagličić, D. Hanžel and D. Lisjak, *Materials Chemistry and Physics* 127 (3), 415-419 (2011).

[77] M. Radwan, M. M. Rashad and M. M. Hessien, *Journal of Materials Processing Technology* 181 (1–3), 106-109 (2007).

[78] J. Liu, P. Liu, X. Zhang, D. Pan, P. Zhang and M. Zhang, *Ultrasonics Sonochemistry* 23, 46-52 (2015).

[79] P. Shepherd, K. K. Mallick and R. J. Green, *Journal of Magnetism and Magnetic Materials* 311 (2), 683-692 (2007).

[80] Munasir, A. Sulton, Triwikantoro, M. Zainuri and Darminto, *AIP Conference Proceedings* 1555 (1), 28-31 (2013).

[81] Munasir, Triwikantoro, M. Zainuri and Darminto, in *Materials Science-Poland* (2015), Vol. 33, pp. 47.

[82] U. Nurbaiti, F. A. Suud, Darminto, Triwikantoro, M. Zainuri and S. Pratapa, *AIP Conference Proceedings* 1710, 030037 (2016).

[83] S. Ammar, K. Ramesh, B. Vengadaesvaran, S. Ramesh and A. K. Arof, *Electrochimica Acta* 220, 417-426 (2016).

[84] S. Ammar, K. Ramesh, I. A. W. Ma, Z. Farah, B. Vengadaesvaran, S. Ramesh and A. K. Arof, *Surface and Coatings Technology* 324, 536-545 (2017).

[85] X. Shi, T. A. Nguyen, Z. Suo, Y. Liu and R. Avci, *Surface and Coatings Technology* 204 (3), 237-245 (2009).

[86] G. Montes-Hernandez, F. Renard, N. Geoffroy, L. Charlet and J. Pironon, *Journal of Crystal Growth* 308 (1), 228-236 (2007).

[87] L. Wang, I. Sondi and E. Matijević, *Journal of Colloid and Interface Science* 218 (2), 545-553 (1999).

[88] E. M. Flaten, M. Seiersten and J.-P. Andreassen, *Journal of Crystal Growth* 312 (7), 953-960 (2010).

[89] Q. Hu, J. Zhang and U. Becker, *MRS Proceedings* 1272, 03-06 (2011).

[90] H. Tao, Y. He and X. Zhao, *Powder Technology* 283, 308-314 (2015).

[91] F. Karakaş and M. S. Çelik, *Progress in Organic Coatings* 74 (3), 555-563 (2012).

[92] D. B. Trushina, T. V. Bukreeva, M. V. Kovalchuk and M. N. Antipina, *Materials Science and Engineering:* C 45, 644-658 (2014).

[93] V. Vergaro, E. Carata, E. Panzarini, F. Baldassare, L. Dini and G. Ciccarella, *AIP Conference Proceedings* 1667 (1), 020014 (2015).

[94] Y. Zhang, P. Ma, Y. Wang, J. Du, Q. Zhou, Z. Zhu, X. Yang and J. Yuan, *World Journal of Nano Science and Engineering* 2 (1), 25-31 (2012).

[95] Q. Zhong, W. Li, X. Su, G. Li, Y. Zhou, S. C. Kundu, J. Yao and Y. Cai, *Colloids and Surfaces B: Biointerfaces* 143, 56-63 (2016).

[96] G. Q. Zheng, X. D. Li, X. M. Wang, J. F. Ma and Z. W. Gu, *Advances in Applied Ceramics* 107 (1), 46-51 (2008).

[97] T. Tsuzuki, K. Pethick and P. G. McCormick, *Journal of Nanoparticle Research* 2 (4), 375-380 (2000).

[98] N. Shimpi, A. Mali, D. P. Hansora and S. Mishra, *Nanoscience and Nanoengineering* 3, 8-12 (2015).

[99] C. Y. Tai and C.-k. Chen, *Chemical Engineering Science* 63 (14), 3632-3642 (2008).

[100] K. Cho, H. Chang, D. S. Kil, B.-G. Kim and H. D. Jang, *Journal of Industrial and Engineering Chemistry* 15 (2), 243-246 (2009).

[101] K. Eguchi, T. Satake, M. Tajika, S. Kuwamoto, K. Yokoyama, J. Matsui, T. Issiki and N. Umesaki, *IOP Conference Series: Materials Science and Engineering* 18 (6), 062001 (2011).

[102] Y. S. Han, G. Hadiko, M. Fuji and M. Takahashi, *Journal of the European Ceramic Society* 26 (4–5), 843-847 (2006).

[103] R. Babou-Kammoe, S. Hamoudi, F. Larachi and K. Belkacemi, *The Canadian Journal of Chemical Engineering* 90 (1), 26-33 (2012).

[104] C. Martos, B. Coto, J. L. Peña, R. Rodríguez, D. Merino-Garcia and G. Pastor, *Journal of Crystal Growth* 312 (19), 2756-2763 (2010).

[105] S. Asaf Kleopas, S. Diwakar, H. J. Heeres and M. Anurag, *Nanotechnology* 18 (3), 035607 (2007).

[106] M. V. Dagaonkar, A. Mehra, R. Jain and H. J. Heeres, *Chemical Engineering Research and Design* 82 (11), 1438-1443 (2004).

[107] J. Chen and L. Xiang, *Powder Technology* 189 (1), 64-69 (2009).

[108] Y. F. Ma, Y. H. Gao and Q. L. Feng, *Journal of Crystal Growth* 312 (21), 3165-3170 (2010).

[109] Z. Chen and Z. Nan, *Journal of Colloid and Interface Science* 358 (2), 416-422 (2011).

[110] Q. Zhang, L. Ren, Y. Sheng, Y. Ji and J. Fu, *Materials Chemistry and Physics* 122 (1), 156-163 (2010).

[111] Y. Zhao, S. Li, L. Yu, Y. Liu, X. Wang and J. Jiao, *Journal of Crystal Growth* 324 (1), 278-283 (2011).

[112] Z. Zhao, L. Zhang, H. Dai, Y. Du, X. Meng, R. Zhang, Y. Liu and J. Deng, *Microporous and Mesoporous Materials* 138 (1–3), 191-199 (2011).

[113] K. N. Islam, M. Z. B. A. Bakar, M. E. Ali, M. Z. B. Hussein, M. M. Noordin, M. Y. Loqman, G. Miah, H. Wahid and U. Hashim, *Powder Technology* 235, 70-75 (2013).

[114] M. Mohamed, N. A. Rashidi, S. Yusup, L. K. Teong, U. Rashid and R. M. Ali, *Journal of Cleaner Production* 37, 394-397 (2012).

[115] Ö. Cizer, C. Rodriguez-Navarro, E. Ruiz-Agudo, J. Elsen, D. Van Gemert and K. Van Balen, *Journal of Materials Science* 47 (16), 6151-6165 (2012).

[116] Z. Arifin, S. Pratapa, Triwikantoro and Darminto, *AIP Conference Proceedings* 1554 (1), 90-92 (2013).

[117] A. Taufiq, Sunaryono, E. G. Rachman Putra, A. Okazawa, I. Watanabe, N. Kojima, S. Pratapa and Darminto, *Journal of Superconductivity and Novel Magnetism* 28 (9), 2855-2863 (2015).

[118] H. Iida, K. Takayanagi, T. Nakanishi and T. Osaka, *Journal of Colloid and Interface Science* 314 (1), 274-280 (2007).

[119] Z. Arifin, A. Riyanto, Q. Lailiyah and S. Pratapa, *Transactions of the Indian Ceramic Society* 74 (4), 202-207 (2015).

[120] G. Thirupathi and R. Singh, *Physica B: Condensed Matter* 448, 346-348 (2014).

[121] G. Paul, P. Kumar Das and I. Manna, *Journal of Magnetism and Magnetic Materials* 404, 29-39 (2016).

[122] A. N. Afifah, S. Syahrullail and N. A. C. Sidik, *Renewable and Sustainable Energy Reviews* 55, 1030-1040 (2016).

[123] A. Katiyar, P. Dhar, T. Nandi and S. K. Das, *Journal of Magnetism and Magnetic Materials* 436, 35-46 (2017).

[124] S. Masoud Hosseini, L. Vafajoo, E. Ghasemi and B. H. Salman, *International Journal of Heat and Mass Transfer* 93, 228-234 (2016).

[125] A. K. Sharma, A. K. Tiwari and A. R. Dixit, *Renewable and Sustainable Energy Reviews* 53, 779-791 (2016).

[126] M. E. Khosroshahi and L. Ghazanfari, *Journal of Magnetism and Magnetic Materials* 324 (24), 4143-4146 (2012).

[127] M. I. Shliomis and K. I. Morozov, *Physics of Fluids* 6 (8), 2855-2861 (1994).

[128] Darminto, M. N. Cholishoh, F. A. Perdana, M. A. Baqiya, Mashuri, Y. Cahyono and Triwikantoro, *AIP Conference Proceedings* 1415 (1), 234-237 (2011).

[129] H. Nikmanesh, M. Moradi, G. H. Bordbar and R. Shams Alam, *Journal of Alloys and Compounds* 708, 99-107 (2017).

[130] D. A. Vinnik, A. S. Semisalova, L. S. Mashkovtseva, A. K. Yakushechkina, S. Nemrava, S. A. Gudkova, D. A. Zherebtsov, N. S. Perov, L. I. Isaenko and R. Niewa, *Materials Chemistry and Physics* 163, 416-420 (2015).

[131] S. S. Seyyed Afghahi, M. Jafarian, M. Salehi and Y. Atassi, Journal of Magnetism and Magnetic Materials 421, 340-348 (2017).

[132] L. S. I. Liyanage, S. Kim, Y.-K. Hong, J.-H. Park, S. C. Erwin and S.-G. Kim, *Journal of Magnetism and Magnetic Materials* 348, 75-81 (2013).

[133] T. Wang, Y. Li, L. Wang, C. Liu, S. Geng, X. Jia, F. Yang, L. Zhang, L. Liu, B. You, X. Ren and H. Yang, *RSC Advances* 5 (74), 60114-60120 (2015).

[134] S. S. S. Afghahi, M. Jafarian, Y. Atassi and C. A. Stergiou, *Materials Chemistry and Physics* 186, 584-591 (2017).

[135] F. Dolatzadeh, S. Moradian and M. M. Jalili, *Corrosion Science* 53 (12), 4248-4257 (2011).

[136] Y. Wen, L. Xiang and Y. Jin, *Materials Letters* 57 (16–17), 2565-2571 (2003).

[137] Z. Nan, Z. Shi, B. Yan, R. Guo and W. Hou, *Journal of Colloid and Interface Science* 317 (1), 77-82 (2008).

[138] A. Olad and A. Rashidzadeh, *Iranian Journal of Chemical Engineering* 5 (2), 45-54 (2008).

[139] R. M. Torresi, S. d. Souza, J. E. P. d. Silva and S. I. C. d. Torresi, *Electrochimica Acta* 50 (11), 2213-2218 (2005).

NANOPOWDERS PRODUCED FROM NATURAL SOURCES USING THE SIMPLE COPRECIPITATION METHOD

ORIGINALITY REPORT

14%	10%	6%	6%
SIMILARITY INDEX	INTERNET SOURCES	PUBLICATIONS	STUDENT PAPERS

PRIMARY SOURCES

1	eprints.oa.edu.ua Internet Source	4%
2	www.conscientiabeam.com Internet Source	2%
3	Malik Anjelh Baqiya, Retno Asih, Muhammad Ghufron, Mastuki, Dwi Yuli Retnowati, Triwikantoro, Darminto. " Ferrite-Based Nanoparticles Synthesized from Natural Iron Sand as the Fe Ion Source ", IntechOpen, 2019 Publication	2%
4	mafiadoc.com Internet Source	1%
5	Submitted to Dominican University Student Paper	1%
6	M C Aisiyah, M Zainuri, D Ristiani. "Magnetic and microwave absorbing properties of Zn-substituted Barium M-Hexaferrite in X-band frequency range", IOP Conference Series: Materials Science and Engineering, 2019 Publication	1%
7	www.intechopen.com Internet Source	1%
8	www.science.gov Internet Source	1%
9	www.worldnanoconference.com Internet Source	1%

10 Submitted to Universiti Putra Malaysia
Student Paper

1%

Exclude quotes	On	Exclude matches	< 1%
Exclude bibliography	On		